Layer Design of Highly Efficient Optically Pumped Semiconductor Disk Lasers

Frank Demaria

A carefully elaborated layer design for optically pumped disk lasers is presented. Its goal is to achieve a high optical conversion efficiency by an effective pump light absorptance and an uniform supply of the multiple quantum wells with carriers generated in the surrounding barriers. Experimental results support the appropriateness of the described approach.

1. Introduction

Optically pumped semiconductor disk lasers (OPSDLs) with extended cavities are surface-emitting laser devices which efficiently convert the low-beam-quality emission of a pump laser to a high-beam-quality circular non-astigmatic laser emission. Furthermore, the extended cavity can be utilized for intra-cavity second harmonic generation by insertion of nonlinear optical crystals. By that way, the range of usable wavelengths is drastically expanded from the near infrared to the visible range of the optical spectrum [1–5].

Like in common semiconductor lasers, the gain of OPSDLs is provided by quantum wells. To obtain sufficient modal gain, in surface emitting lasers, multiple quantum wells are positioned in a way that supports a lasing field intensity with its antinodes as close as possible to the wells. This is usually realized by a periodical gain structure wherein a series of quantum wells is spaced at an optical distance of half the design wavelength [6]. The composition of the quantum wells ideally determines the peak-gain wavelength in laser operation which fits the design wavelength. Such a structure was also implemented in the pioneering OPSDLs of Kuznetsov et al. [7] where it was combined with an epitiaxially-grown back-side Bragg reflector having its stopband centered near the emission wavelength. However, without any further design features, the carrier generation rate in the barriers of the lower quantum wells of such a single-pass pump-light-absorbing structure suffers from the decay of the pump intensity resulting from the absorption in the barriers of the upper quantum wells. This is unfavorable, as high optical conversion efficiencies and slope efficiencies require a uniform distribution of the carriers over the quantum wells [8]. One possible design strategy which can be pursued to overcome this is to separate the gain structure and the absorbing barriers into sections with unequal absorbing volumes and (or) an unequal number of quantum wells to establish approximately constant carrier generation per well [9]. Our approach which shall be described here is different. It consequently takes advantage from the implementation of a back-side double-band Bragg reflector (DBBR) which provides not only high reflectivity for the actual laser resonance but also for the incident pump beam. That way, in combination with the reflecting surface

interfaces of the laser chip, a Fabry-Pérot microcavity is established also for the pump light which supports high absorptance. This also leads to an uniform carrier distribution over the quantum wells and thus highest conversion efficiencies.

2. Layer Design

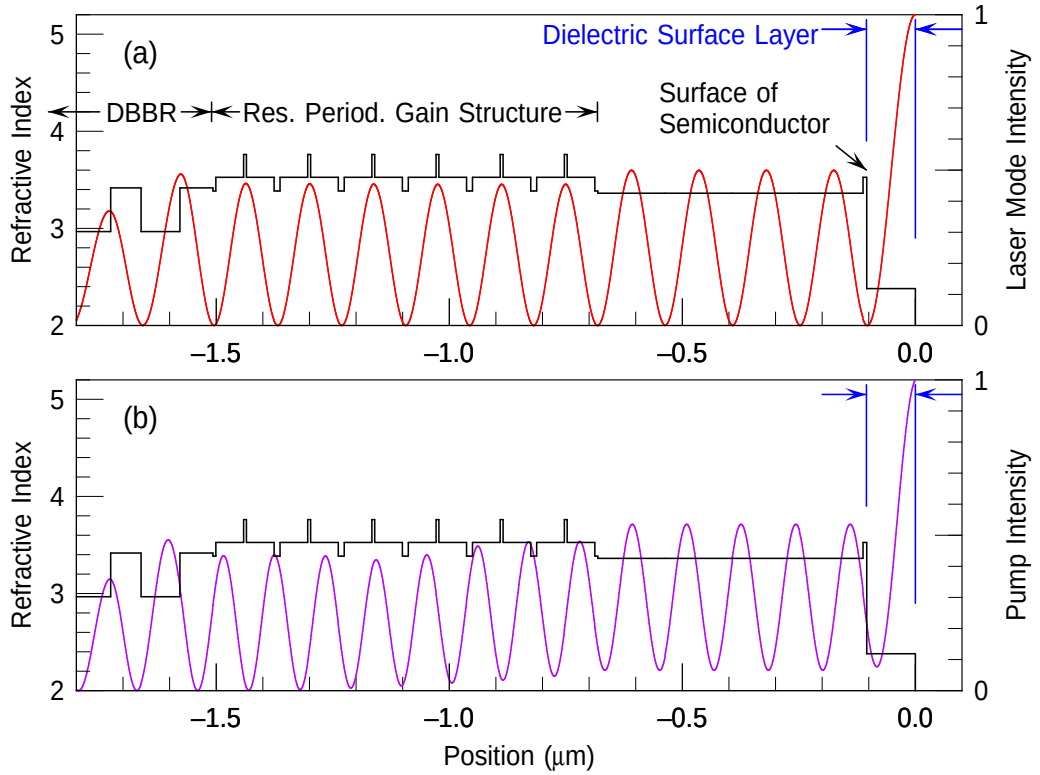

Fig. 1: Design of the top region of the semiconductor disk laser, visualized by the index of refraction, beginning from the surface layer on the right side to the first layers of the rear DBBR on the left. In (a), the electric field intensity for the design wavelength $\lambda_e = 980\,\text{nm}$ in case of perpendicular propagation is shown and in (b) for unpolarized pump radiation with a wavelength $\lambda_p = 808\,\text{nm}$ at an angle of incidence $\theta_i = 25°$.

Figure 1 shows the top region of a OPSDL layer structure, represented by the index of refraction. It is designed for an emission wavelength of $\lambda_e = 980\,\text{nm}$ and for pumping with a wavelength of $\lambda_p = 808\,\text{nm}$ under an angle of incidence $\theta_i = 25°$. The structure consists of the following functional regions:

- *Surface Layer:* The semiconductor structure is covered by a dielectric TiO_2 coating with the optical thickness of $\lambda_e/4$.
- *Resonant Periodic Gain (RPG) Structure:* Six 6.2 nm-thick $In_{0.155}Ga_{0.845}As$–GaAs quantum wells are arranged at a distance that corresponds to an optical thickness of $\lambda_e/2$. Strain compensation is realized by $GaAs_{0.74}P_{0.26}$ layers which are located at a central position between the QWs and at the boundaries of the structure. These

layers have a higher bandgap as the surrounding barriers and therefore also act as carrier diffusion barriers.

- *Rear Reflector:* 66 epitaxially-grown layers build up the double-band Bragg reflector which is supported by the rear metallization. The structure is numerically optimized to provide high reflectivity at the emission wavelength as well as for the pump light. The spectral reflectivity function which is shown in Fig. 2 was calculated by the matrix formulation for isotropic layered media and monochromatic plane waves [11].

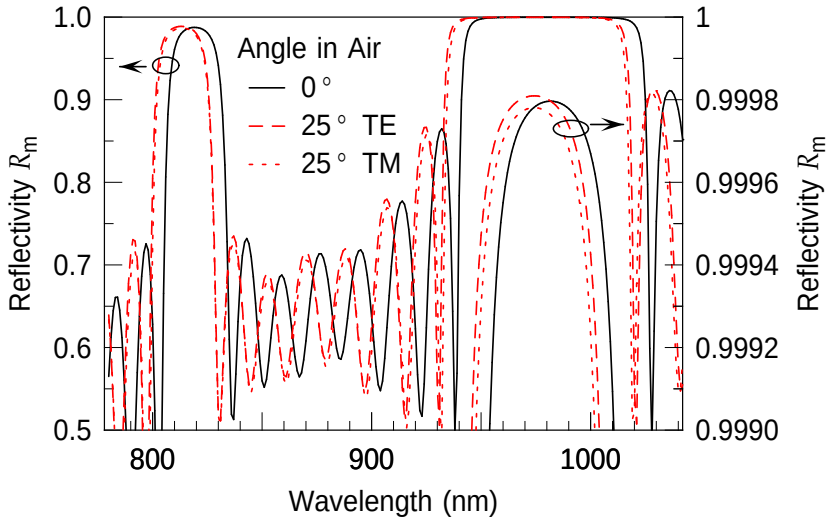

Fig. 2: Calculated internal reflectivities of the DBBR in combination with the rear metalization for normal incidence ($\theta_i = 0°$) and an incidence angle of $\theta_i = 25\,°$.

The dielectric surface layer results in a reflectivity of 6 % at 980 nm and 8 % for unpolarized 808 nm pump radiation at an incident angle of $\theta_i = 25°$. Hence, an internal cavity with a length of few microns is established in combination with the DBBR for both the pump and emission wavelength. On the wavelength scale of the internal cavity's Fabry-Pérot resonances, the mode spectrum of the extended cavity becomes quasi-continuous because the distance of the external mirror exceeds the internal cavity length by an order of at least three magnitudes. For this reason the influence of the extended cavity on the field distribution of the resonant laser mode can be neglected, even though in principle a three-mirror cavity has to be considered. The emitting resonance in Fig. 1 (a) shows antinodes at the QW positions and at the surface of the structure. The surface of the semiconductor is located at the interface to the dielectric surface layer at $x \approx$-0.105 µm, where a node of the field is located.

Also, the pump resonance in Fig. 1 (b) exhibits a minimum close to the semiconductor surface which leads to a reduced absorption in that region. This design strategy was also applied to a disk laser which was designed for direct pumping of the QWs and led to high efficient emission at wavelengths around 860 nm [12]. Unlike the emitting resonance, the standing wave pattern of the resonant pump intensity is significantly superimposed by a ground level, which decreases towards the DBBR. This is due to the fraction of pump

energy which is absorbed in the QWs and the surrounding barriers. However, compared to single-pass pump light absorbing structures, the contribution of the periodic fraction which is built up by the resonant reflection at the DBBR and the surface layer of the structure is much higher and results in a much more homogeneous pumping of the QWs. The efficient and homogeneous supply of the QWs with carriers that are generated in the barriers by the pump intensity is also supported by the high-bandgap strain compensation layers which are located in the center between the QWs and at the edges of the RPG structure. They define a clear direction of the longitudinal diffusion and confine the absorbing volume which provides the embedded QW with carriers. The thickness of the absorbing volume equals the distance between two QWs reduced by the thickness of the strain compensation layers, thereby it is adapted to the periodicity of the pump intensity distribution. The overall carrier generation rate of the absorbing volume which supports one QW is approximately proportional to the integral of the pump intensity distribution over its thickness. This results in a decoupling of the pump rate and the phase of the periodic fraction of the pump field for a single QW since the definite integral over one period is independent from the position of the maximum within the boundaries.

3. Device Fabrication and Mounting

The layer structure has been grown by molecular beam epitaxy on GaAs substrate. The direction of growth is reverse to the laser emission. Hence, the wafer structure ends with the DBBR on top. On top of the DBBR, a metalization layer is applied for proper soldering and reflectivity enhancement. To facilitate the fabrication of laser chips with a size of $1.2 \times 1.7\,\mathrm{mm}^2$ by cleaving, the substrate is thinned to a thickness of approximately $140\,\mu\mathrm{m}$ by wet chemical polishing. The chips are then bonded upside-down onto 3-mm-thick gold-plated copper heat spreaders or with 0.3-mm-thick diamond heat spreaders onto microchannel heat sinks for water cooling [10]. This approach allows entire substrate removal and efficient heat extraction by extra-cavity heat spreaders. After the residual substrate has been removed by selective wet chemical etching, the surface layer is applied by ion-beam sputter depositionin a final fabrication step.

4. Reflectivity Spectra

Valuable information on the performance of layer designs and realized OPSDL structures can be extracted from calculated and measured reflectivity spectra. Also, the performance of isolated components of the structure can be calculated to support a modular construction approach. An example is given by the reflectivity spectrum of an isolated DBBR in Fig. 2. It also shows clearly how the spectral characteristics is shifted towards shorter wavelengths for an increasing angle of incidence. This has to be considered as the angle of the incident pump beam differs from the direction of emission at large.

Reflectivity spectra of a whole OPSDL structure are shown in Fig. 3, for an incidence angle $\theta_\mathrm{i} = 5\,^\circ$ at room temperature. For comparison measured and calculated curves are plotted. The calculations where performed for different wavelength ranges by the same method as for the rear reflector in Fig. 2.

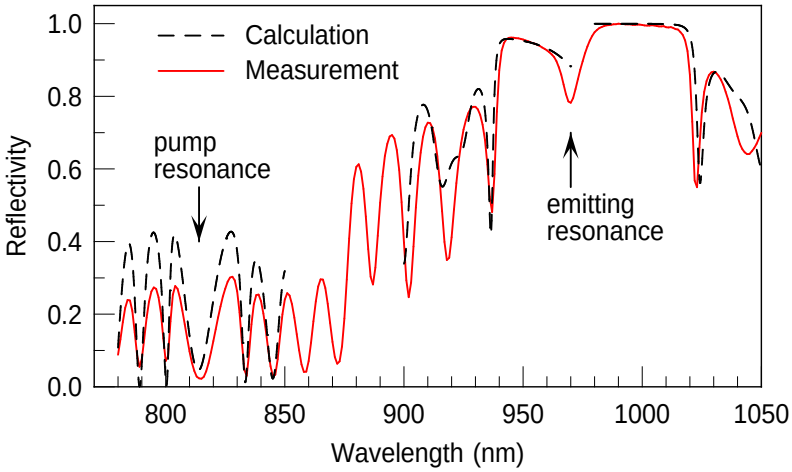

Fig. 3: Measured and calculated reflectivity spectra of the whole structure at an incidence angle $\theta_i = 5\,°$.

For 780–850 nm, a constant absorption coefficient of 9500 cm^{-1} is assumed for the QWs and the surrounding barriers as well as 9000 cm^{-1} for the 8 nm-thick GaAs anti-oxidation layer. For 900–970 nm only the QWs have been taken into account with an absorption of 6800 cm^{-1}. Above 980 nm no absorption is considered. The mentioned values have been extracted from the graphical representation of gain calculations, performed by Corzine et al. [13].

Both, measurement and calculation reveal distinct dips at the labeled positions at 813 nm and 970 nm which originate from resonant absorption in the laser's Fabry-Pérot microcavity. Often, within the long wavelength stop-band, two different reflectivity dips can be distinguished, originating from the resonance of the microcavity and the absorption peak of the QWs which is related to the gain peak in laser operation [3, 14]. Here, both peaks overlap at room temperature giving evidence that the resonance of the microcavity and the maximum of the gain spectrum are matched.

For an incident angle of about 25 °, the pump resonance shifts to a value that equals the pump wavelength of about 808 nm. By means of adjusting the angle of incidence, absorptance values up to 96 % have been achieved for 805 nm pump wavelength with 3 nm linewidth (10 dB drop). Comparison with Fig. 2 shows that the pump resonance is located in the center of the short wavelength stopband where maximum reflectivity is provided. Hence the absorption of the pump light takes place nearly exclusively in the designated regions, which are rather the QWs and their surrounding barriers than the metalization underneath the DBBR.

5. Output Characteristics

The output power and absorption characteristics of the device with the reflectivity spectrum presented in Fig. 3 are shown in Fig. 4. In this case the laser chip was mounted on a water-cooled microchannel heat sink with a 0.3 mm-thick diamond heat spreader in between. An extended cavity with a simple hemispherical resonator configuration was

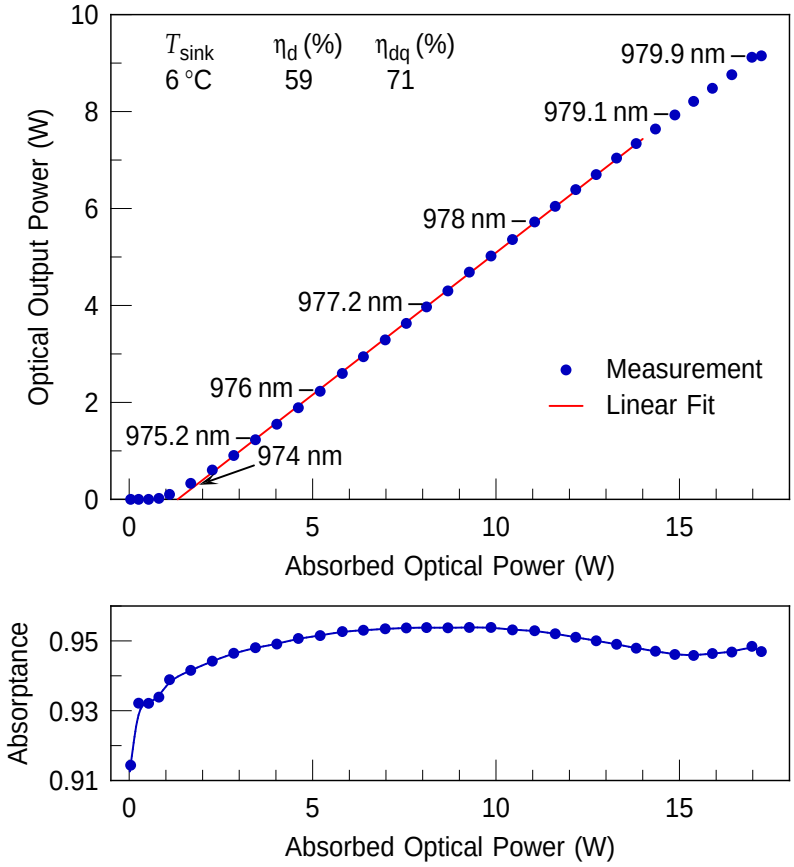

Fig. 4: The upper graph shows the measured output characteristics versus absorbed pump power of the laser device with the reflectivity spectrum shown in Fig. 3. The related absorption efficiency is shown in the lower graph. To achieve sufficient cooling, the laser chip is mounted on a water cooled microchannel heat sink with a 0.3 mm-thick diamond heat spreader and a temperature of the cooling water T_{sink}. Also shown are the extracted slope conversion efficiency η_d and the differential quantum efficiency η_{dq}. Some measurement points are labeled with the emission wavelength.

established by an external mirror of $R_c = 100$ mm radius of curvature and 3.6 % transmittance for the emission wavelength. The laser was pumped at an angle of 28 ° with a pump-spot area of 310 µm × 330 µm. With increasing pump power, the temperature of the OPSDL structure increases and therefore the reflectivity spectrum is displaced towards longer wavelengths. The maximum absorptance of over 95 % is achieved at a pump power of about 9 W for which the minimum of the Fabry-Pérot resonance dip of the microcavity overlaps with the pump wavelength of 808 nm. At an incident pump power of 17.9 W, a fraction of 17.2 W is absorbed and an optical power of 9.1 W is emitted. This corresponds to conversion efficiencies of 51 % and 53 %. From the linear fit of the curve a slope efficiency of 59 % can be extracted which corresponds to a differential quantum efficiency of 71 %. A similar structure which was mounted on simple gold-plated copper heat sinks led to an output power of 13.2 W at a heat sink temperature of -5 °C [15]. The related conversion efficiency is 54 % referred to the absorbed pump power and a differential quantum efficiency of 73 % has been achieved.

6. Conclusion

A layer design for OPSDLs that leads to optimized longitudinal field distributions of the resonantly pumped devices has been described. The approach is substantiated by experimental results from such devices which reveal the highest absorption efficiency, conversion efficiency, and differential quantum efficiencies which so far have been reported for OPSDLs to the best knowledge of the author.

References

[1] E. Schielen, M. Golling, and P. Unger, "Diode-pumped semiconductor disk laser with intracavity frequency doubling using lithium triborate (LBO)," *IEEE Photon. Technol. Lett.*, vol. 14, no. 6, pp. 777–779, 2005.

[2] E. Gerster, I. Ecker, S. Lorch, C. Hahn, S. Menzel, and P. Unger, "Orange-emitting frequency-doubled GaAsSb/GaAs semiconductor disk laser," *J. Appl. Phys.*, vol. 94, no. 12, pp. 7397–7401, 2003.

[3] J.-Y. Kim, S. Cho, J. Lee, G. B. Kim, S.-J. Lim, J. Yoo, K.-S. Kim, S.-M. Lee, J. Shim, T. Kim, and Y. Park, "A measurement of modal gain profile and its effect on the lasing performance in vertical-external-cavity surface-emitting lasers," *IEEE Photon. Technol. Lett.*, vol. 18, no. 23, pp. 2496–2498, 2006.

[4] J. Rautiainen, A. Härkönen, V.-M. Korpijärvi, P. Tuomisto, M. Guina, and O. G. Okhotnikov, "2.7 W tunable orange-red GaInNAs semiconductor disk laser," *Opt. Express*, vol. 15, no. 26, pp. 18 345–18 350, 2007.

[5] M. Fallahi, L. Fan, Y. Kaneda, C. Hessenius, J. Hader, H. Li, J. Moloney, B. Kunert, W. Stolz, S. Koch, J. Murray, and R. Bedford, "5-w yellow laser by intracavity frequency doubling of high-power vertical-external-cavity surface-emitting laser," *IEEE Photon. Technol. Lett.*, vol. 20, no. 20, pp. 1700–1702, 2008.

[6] M. Y. A. Raja, S. R. J. Brueck, M. Osiński, C. F. Schaus, J. G. McInerney, T. N. Brennan, and B. E. Hammons, "Resonant periodic gain surface-emitting semiconductor lasers," *IEEE J. Quantum Electron.* **25**, pp. 1500–1512, 1989.

[7] M. Kuznetsov, F. Hakimi, R. Sprague, and A. Mooradian, "High-power >0.5-W cw diode-pumped vertical-external-cavity surface-emitting semiconductor lasers with circular TEM_{00} beams," *IEEE Photon. Technol. Lett.*, vol. 9, no. 8, pp. 1063–1065, 1997.

[8] O. Casel, *Experimentelle Untersuchung und Modellierung des Einflusses der Epitaxiestruktur auf die physikalischen Eigenschaften optisch angeregter Halbleiterscheibenlaser*. Ph.D. thesis, University of Kaiserslautern, Göttingen: Culliver, 2005.

[9] S. Giet, H.D. Sun, S. Calvez, M.D. Dawson, S. Suomalainen, A. Harkonen, M. Guina, O. Okhotnikov, and M. Pessa, "Spectral narrowing and locking of a vertical-external-cavity surface-emitting laser using an intracavity volume Bragg grating," *IEEE Photon. Technol. Lett.*, vol. 18, no. 16, pp. 1786–1788, 2006.

[10] E. Gerster, "Semiconductor Disk Laser on Microchannel Cooler," *Annual Report 2004*, pp. 79–84, Ulm University, Institute of Optoelectronics.

[11] P. Yeh, *Optical Waves in Layered Media*, John Wiley & Sons, 1988.

[12] S.-S. Beyertt, F. Demaria, U. Brauch, N. Dhidah, A. Giesen, T. Kübler, S. Lorch, F. Rinaldi, and P. Unger, "Efficient gallium-arsenide disk laser," *IEEE J. Quantum Electron.*, vol. 43, no. 10, pp. 869–875, 2007.

[13] S. W. Corzine, R.-Y. Yan, and L. A. Coldren, "Optical gain in III-V bulk and quantum well semiconducors," in P. S. Zory, Jr. (Editor), *Quantum Well Lasers, Quantum Electronics–Principles and Appications*, Academic Press Inc., San Diego, 1993.

[14] S. Cho, G. B. Kim, J.-Y. Kim, K.-S. Kim, S.-M. Lee, J. Yoo, T. Kim, and Y. Park, "Compact and efficient green VECSEL based on novel optical end-pumping scheme," *IEEE Photon. Technol. Lett.*, vol. 19, no. 17, pp. 1325–1327, 2007.

[15] F. Demaria, S. Lorch, S. Menzel, M. C. Riedl, F. Rinaldi, R. Rösch, and P. Unger, "Design of highly-efficient high-power optically-pumped semiconductor disk lasers," accepted for publication in *IEEE J. Select. Topics Quantum Electron*, May/June, 2009.